


Electron Slingshot Acceleration in Relativistic Preturbulent Shocks Explored via Emitted Photon Polarization

Zheng Gong^{⊗,*}, Xiaofei Shen[⊗], Karen Z. Hatsagortsyan^{⊗,†} and Christoph H. Keitel[⊗]
Max-Planck-Institut für Kernphysik, Saupfercheckweg 1, 69117 Heidelberg, Germany

 (Received 23 May 2023; revised 23 September 2023; accepted 23 October 2023; published 29 November 2023)

Transient electron dynamics near the interface of counterstreaming plasmas at the onset of a relativistic collisionless shock (RCS) is investigated using particle-in-cell simulations. We identify a slingshotlike injection process induced by the drifting electric field sustained by the flowing focus of backward-moving electrons, which is distinct from the well-known stochastic acceleration. The flowing focus signifies the plasma kinetic transition from a preturbulent laminar motion to a chaotic turbulence. We find a characteristic correlation between the electron dynamics in the slingshot acceleration and the photon emission features. In particular, the integrated radiation from the RCS exhibits a counterintuitive nonmonotonic dependence of the photon polarization degree on the photon energy, which originates from a polarization degradation of relatively high-energy photons emitted by the slingshot-injected electrons. Our results demonstrate the potential of photon polarization as an essential information source in exploring intricate transient dynamics in RCSs with relevance for Earth-based plasma and astrophysical scenarios.

DOI: [10.1103/PhysRevLett.131.225101](https://doi.org/10.1103/PhysRevLett.131.225101)

Plasma shocks are characterized by rapid steepening of a nonlinear wave, the eventual overtaking by its rear part, and the irreversible energy transfer to the surrounding particles [1–3]. They are of extensive interest in various scenarios. In the laboratory, a nonrelativistic shock can generate multi-MeV ions in plasma-based accelerators [4–9], improve the thermonuclear gain of inertial confinement fusion [10–13], and provide a platform for investigating astrophysical phenomena [14–20]. For astrophysics, the shock formed by supernova remnants offers plausible mechanisms toward understanding the origin of TeV cosmic leptons [21–24] and galactic PeVatrons [25], while relativistic collisionless shocks (RCSs) are ubiquitous in pulsar wind nebulae [26], active galactic nuclei [27], and gamma-ray bursts (GRBs) [28]. Recent observations suggest that the RCS-prompted afterglow radiation indicates a peculiar long GRB from the merger of a compact binary system [29–32] rather than the core collapse of massive stars [33], which restimulates the research interest of relevant RCSs [34].

The RCS brewed from GRBs is prone to load with e^\pm pairs, since the γ -ray photons ahead of the GRB ejecta turn into e^\pm via γ - γ reaction [35–37]. Meanwhile, the magnetization level of the unshocked interstellar medium is so low that the unmagnetized initial condition is generally

considered [38]. Here, the magnetized filamentation turbulence, self-generated through the filamentation merging and magnetic loop coalescence [39–46], is crucial for determining Weibel-mediated shock microstructures [47–54], where electrons, undergoing severe swirling and trace crossing, no longer travel in a quasilayer form. The electrons might experience stochastic acceleration, akin to the Fermi process [55,56], which has been well recognized as sources of energetic electrons in the Universe [57–67]. Previous studies of unmagnetized RCSs primarily focus on the electron energization and equipartition between electrons and ions through stochastic acceleration [68–72] where electrons scatter off the self-generated turbulent magnetic structures [73–75]. However, it remains largely unexplored how the plasma transits from the nonturbulent flow to kinetic turbulence and how this transition impacts the acceleration and radiation features in the RCS.

As a versatile information carrier of multimessenger astrophysics [76–78], photon polarization is critical for measuring the magnetic configuration near black holes [79] and crab nebulae [80]. Therefore, the question arises whether the polarization feature of spontaneously emitted photons can be employed to reveal the mechanism responsible for the turbulence transition in a RCS.

In this Letter, we investigate the transient electron dynamics in the transition to turbulence near the counterstreaming interface of an unmagnetized pair-loaded RCS precursor, which is potentially associated with the outflow of GRBs. We employ particle-in-cell (PIC) simulations to examine the photon emission and observe an anomalous nonmonotonic dependence (NMD) of the photon

Published by the American Physical Society under the terms of the Creative Commons Attribution 4.0 International license. Further distribution of this work must maintain attribution to the author(s) and the published article's title, journal citation, and DOI. Open access publication funded by the Max Planck Society.

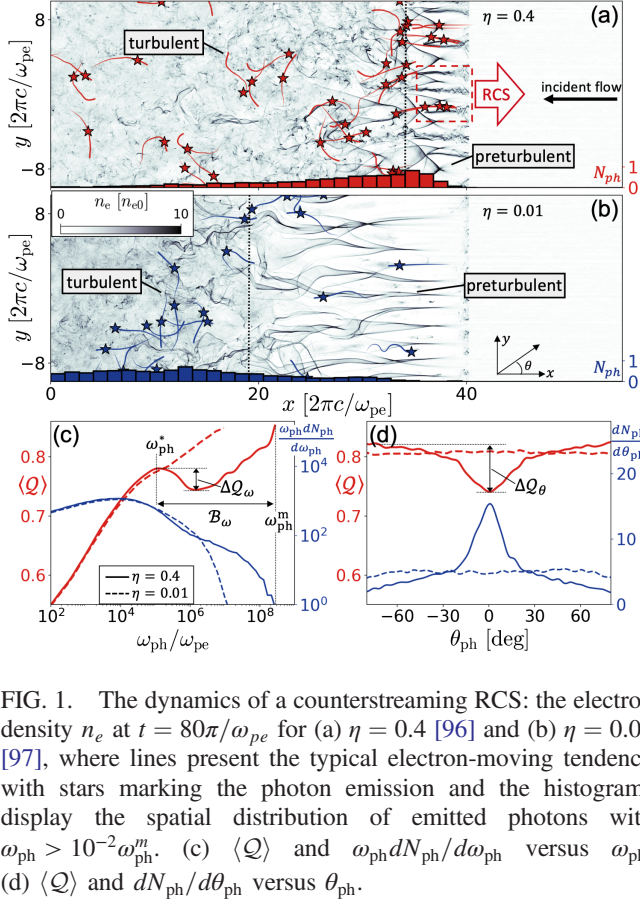


FIG. 1. The dynamics of a counterstreaming RCS: the electron density n_e at $t = 80\pi/\omega_{pe}$ for (a) $\eta = 0.4$ [96] and (b) $\eta = 0.01$ [97], where lines present the typical electron-moving tendency with stars marking the photon emission and the histograms display the spatial distribution of emitted photons with $\omega_{ph} > 10^{-2}\omega_{ph}^m$. (c) $\langle Q \rangle$ and $\omega_{ph}dN_{ph}/d\omega_{ph}$ versus ω_{ph} . (d) $\langle Q \rangle$ and $dN_{ph}/d\theta_{ph}$ versus θ_{ph} .

polarization degree on the photon energy. We found that the NMD indicates a specific mechanism of electron acceleration, which we term as slingshot injection, caused by a drifting electric field due to the flowing focus of backward-moving electrons. Our slingshot model could be the essential reason accounting for the long-term directed electron heating via electric fields near a RCS precursor [81–83]. Utilizing Hamiltonian analyses, we elucidate that the backward-flowing focus marks the plasma transition to a turbulent regime in the RCS, which in the electron’s transverse phase space is exhibited as the change from the phase-locked to the phase-slipping dynamics. The NMD photon properties stem from a polarization degradation of relatively high-energy photons emitted by the slingshot-injected electrons. The correlation among the NMD of photon polarization, the slingshot injection, and the backward-flowing focus emphasizes the importance of the transition region to the turbulence in characterizing the acceleration and radiation in the RCS.

We have carried out 2D simulations of counterstreaming RCSs; see Fig. 1. The latter is initiated when a uniform plasma flow with a bulk Lorentz factor $\gamma_0 = 50$, injected from the right side, is reflected from the left side boundary, which adopts a reflection condition [58]. The periodic boundary condition is set in the lateral direction. We consider the flow consisting of electrons, positrons, and

ions with the same drifting velocity and with the number density of n_{e0} , n_{p0} , and n_{i0} , respectively. The charge neutralization $n_{e0} = n_{p0} + Z_i n_{i0}$ is satisfied initially, and the ion with charge (mass) $Z_i = 1$ ($m_i = 1836m_e$) is used. The ratio $\eta \equiv n_{i0}/(n_{i0} + n_{p0}) \in (0.01, 1)$ denotes the proportion of ions among the whole positive charged particles. The simulation domain is $200\lambda_{pe} \times 20\lambda_{pe}$ with resolution $\Delta x = \Delta y = \lambda_{pe}/50$ and $\Delta t = 0.95\Delta x/c$. Each cell is filled with 48 macroparticles for each species. Here, $\omega_{pe} = (n_{e0}e^2/\epsilon_0 m_e)^{1/2}$ ($\lambda_{pe} = 2\pi c/\omega_{pe}$) is the plasma frequency (skin depth), with the electron charge (mass) e (m_e), the vacuum permittivity ϵ_0 , and the speed of light c . The models of the photon polarization have been implemented in the EPOCH code [84,85]. Unless otherwise indicated, we discuss results from the fiducial simulation with $\gamma_0 = 50$ and $\eta = 0.4$.

The snapshot of the electron density n_e in Fig. 1(a) exhibits that the filamentation exclusively exists at the front of the RCS interface. Between two adjacent filaments, an electron focusing point emerges, and, following that, two oblique density strips stretch out [see Fig. 2(b)]. Behind the strips, the coherent filaments and focusing points disappear while the turbulence shows up. A nontrivial thing is that the photons with energy $\epsilon_{ph} \equiv \hbar\omega_{ph} > 10^{-2}\hbar\omega_{ph}^m$ are primarily emitted by electrons near the interface, where $\omega_{ph}^m \sim 10^8\omega_{pe}$ is the photon cutoff frequency and \hbar the Planck constant. In contrast, in the case of $\eta = 0.01$, the energetic photon emission predominantly occurs in the turbulent region [see Fig. 1(b)], even though the preturbulent structures are extended to a larger range.

The degree of the photon’s linear polarization along the direction of the electron’s transverse acceleration is characterized by the Stokes parameter Q [101], formulated as [85]

$$Q = \frac{\epsilon_e(\epsilon_e - \epsilon_{ph})K_{2/3}(\zeta)}{[\epsilon_e^2 + (\epsilon_e - \epsilon_{ph})^2]K_{2/3}(\zeta) - \epsilon_e(\epsilon_e - \epsilon_{ph})\tilde{K}_{1/3}(\zeta)}, \quad (1)$$

where $K_n(\zeta)$ is the modified secondary Bessel function, $\tilde{K}_{1/3}(\zeta) = \int_{\zeta}^{\infty} K_{1/3}(z)dz$, $\zeta = 2\epsilon_{ph}/[3\chi_e(\epsilon_e - \epsilon_{ph})]$, and $\epsilon_e = \gamma_e m_e c^2$ the electron energy; $\chi_e \equiv (e\hbar/m_e^3 c^4)|F_{\mu\nu}p^\nu|$ is the electron quantum strong-field parameter with the field tensor $F_{\mu\nu}$ and the electron four-momentum p^ν . At $\chi_e \ll 0.1$, $\partial Q/\partial \epsilon_{ph} > 0$ predicted by Eq. (1) manifests a monotonic dependence of Q on ω_{ph} , because for the higher-frequency radiation the formation length is shorter and the preservation of the local polarization degree is improved. This monotonic dependence is confirmed by the results of $\eta = 0.01$ [see Figs. 1(c) and 1(d)], where electrons experience stochastic acceleration [59] and the photon emission is isotropic in the angular space. However, for $\eta = 0.4$ [see Figs. 1(c) and 1(d)], the averaged polarization degree $\langle Q \rangle$ versus ω_{ph} exhibits NMD, with a

polarization dip $\Delta Q_\omega \approx 4.5\%$ and a bandwidth ratio $B_\omega \equiv \omega_{\text{ph}}^m / \omega_{\text{ph}}^* \sim 10^3$, contradictory to the forementioned monotonic dependence. Here, ω_{ph}^* is the local maximum point of the function $\langle Q \rangle$ versus ω_{ph} [see Fig. 1(c)]. In the angular distribution, $\langle Q \rangle$ has a polarization valley $\Delta Q_\theta \approx 11\%$, and the photon emission tends to be more collimated within an emission angle $\theta_{\text{ph}} \lesssim 15^\circ$. The features of the slingshot acceleration and the photon NMD are confirmed by 3D PIC simulations [85].

To unveil the reason of the counterintuitive NMD, we focus on the electron dynamics within the dashed box marked in Fig. 1(a). For the deflection of backward-moving electrons nearby the interface, the effective plasma density approximates ηn_{e0} and the charge density has a sinusoidal profile $\rho \sim |e|\eta n_{e0} \cos[k_y(y - y_c)]$ with $k_y \sim \omega_{pe}/2c$ the periodic wave number and y_c the relative central axis [85]. The self-generated transverse electric and magnetic field is $E_y(y) = (|e|\eta n_{e0}/\epsilon_0 k_y) \sin[k_y(y - y_c)]$ and $B_z(y) = cE_y$, respectively. As justified by simulations, the energy exchange $d\gamma_e/dt$ is insignificant, and, thus, the transverse dynamics is described by $\ddot{y} + (\Omega^2/k_y) \sin[k_y(y - y_c)] = 0$, with $\Omega^2 = 2\eta n_{e0} e^2 / \epsilon_0 \gamma_0 m_e$. Then the corresponding Hamiltonian can be derived as [85]

$$H_\perp(y, \dot{y}) = \frac{\Omega^2}{k_y^2} \cos[k_y(y - y_c)] + \frac{1}{2} \dot{y}^2. \quad (2)$$

Following $H_\perp(y, \dot{y}) = H_\perp(y_0, 0)$, the electron transverse motion is analyzed as

$$t = \frac{k_y}{\sqrt{2}\Omega} \int \frac{dy}{\sqrt{\cos[k_y(y_0 - y_c)] - \cos[k_y(y - y_c)]}}. \quad (3)$$

The trajectories predicted by Eq. (3) demonstrate that the backward-moving electrons would be focused into $y = y_c$ at a restoring time $t_r \sim 0.6\pi/\Omega$, as confirmed by simulation results [see Figs. 2(a) and 2(b)].

After the backward-flowing focus, the electrons start to transit from the preturbulent motion to turbulence, interpreted as a shrinking of the Hamiltonian's separatrix. The separatrix $H_\perp(y, \dot{y}) \equiv H_\perp(y_c, 0) = \Omega^2/k_y^2$ divides the electron dynamics into the confined phase-locked and the escaping phase-slippage regions. If the magnetic field decreases with the equivalent restoring frequency reduced from Ω to Ω' , the phase space volume encompassed by the separatrix is shrunk from $H_\perp(y, \dot{y}) < \Omega^2/k_y^2$ to $H_\perp(y, \dot{y}) < \Omega'^2/k_y^2$. Thus, the electrons within the region of $\Omega'^2/k_y^2 < H_\perp(y, \dot{y}) < \Omega^2/k_y^2$ are released into the phase-slippage region [see Fig. 2(c)]. The electron release breaks the coherent filament structure and deteriorates the transverse inhomogeneity, leading to the onset of the plasma turbulence.

The transition from the preturbulent flowing focus to the turbulence is illustrated by the evolution of the particle

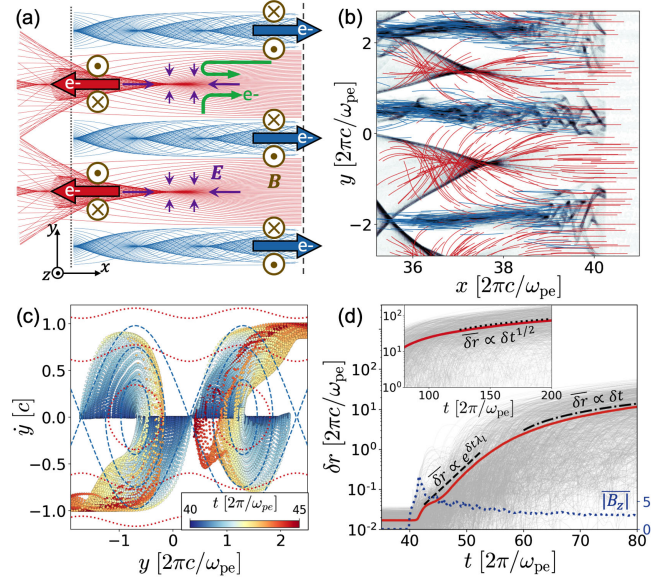


FIG. 2. (a) Schematic of the backward-flowing focus with the predicted electron trajectories [98]. The brown (purple) markers denote the magnetic (electric) field direction, and the green arrows present the slingshot-injected electrons. (b) Enlargement of the dashed box marked in Fig. 1(a), where the red (blue) lines represent the backward- (forward-) moving electrons [99]. (c) Electron evolution in (y, \dot{y}) space with the blue dashed (red dotted) lines contouring $H_\perp|_{\Omega \approx 0.1\omega_{pe}}$ ($H_\perp|_{\Omega' \approx 0.02\omega_{pe}}$) [100]. (d) Time evolution of δr ($\overline{\delta r}$) in gray (red).

separation [see Fig. 2(d)], where δr is the distance between an electron and its closest partner at the beginning and $\overline{\delta r}$ refers to the averaged value. After the focus at $\omega_{pe}t/2\pi \sim 45$, the signature of the chaotic dynamics arises with $\overline{\delta r} \propto \exp(\lambda_l \delta t)$ characterized by the Lyapunov exponent $\lambda_l \approx 0.15\omega_{pe}/\pi$ [102]. The electrons exhibit a chaotic behavior during the defocusing stage [103], where the decrease of the exerted magnetic field $|\overline{B_z}|$ proves the shrinking of the Hamiltonian's separatrix. Later, at $\omega_{pe}t/2\pi \sim 70$, $\overline{\delta r} \propto 0.2c\delta t/\pi$ implies a drifting tendency because of the localized electrons prone to occupy the whole interaction domain [104]. Eventually, at $\omega_{pe}t/2\pi > 130$, $\overline{\delta r} \propto 9(\omega_{pe}\delta t/2\pi)^{1/2}$ manifests the electrons' random walk procedure [105,106].

The flowing focus leads to a negative longitudinal electric field E_x with a scale length δl [see Fig. 3(a)], favorable for injecting electrons into the RCS. This injection resembles a slingshot, where the filaments serve as the handhold, the backward-moving electrons behave as the elastic string, and the injected forward-moving electrons are the projectiles [107]. The scale length is calculated as $\delta l \sim t_r c \approx \pi\sqrt{\gamma_0/\eta}(c/\omega_{pe})$. Given $\nabla \cdot \mathbf{E} = \rho/\epsilon_0$, the field strength is estimated as $\langle E_x \rangle \approx \pi\sqrt{\eta\gamma_0}m_e c \omega_{pe}/|e|$ [see Fig. 3(b)]. The flowing focus successively occurs for the replenished backward-moving electrons, and the field E_x propagates

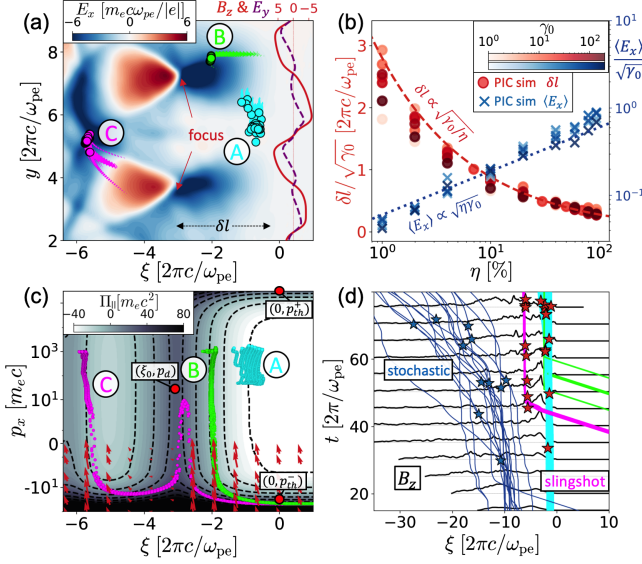


FIG. 3. (a) Electric field E_x with the transverse profile of B_z and E_y . (b) δl and $\langle E_x \rangle$ versus η . (c) Hamiltonian $\Pi_{||}(\xi, p_x)$ with the red arrows denoting the moving tendency modified by the magnetic deflection. (d) Time-evolved electron position, where the black lines profile B_z and the red (blue) stars mark the photon emission belong to the slingshot (stochastic) mechanism. Three kinds of slingshot electrons are shown with the color of (A) cyan, (B) lime, and (C) magenta.

with a velocity $v_x \approx v_d = (1 - 1/\gamma_0^2)^{1/2}$. In the interface's comoving frame $\xi \equiv x - v_d t$, the electron's longitudinal dynamics is determined by the Hamiltonian $\Pi_{||}(\xi, p_x) = -|e|\varphi(\xi) + c\sqrt{m_e^2 c^2 + p_x^2} - v_d p_x$ with $\varphi(\xi) = -\int E_x(\xi) d\xi$ [see Fig. 3(c)] [85]. Then the injection threshold p_{th}^- and the maximum achievable momentum p_{th}^+ , derived as [85]

$$p_{\text{th}}^+ \sim 2\gamma_0^3 + \frac{3}{2}\gamma_0 - \frac{2}{\gamma_0} \quad \text{and} \quad p_{\text{th}}^- \sim -\frac{\gamma_0}{2} - \frac{1}{2\gamma_0}. \quad (4)$$

Specifically, there are three types of slingshot-injected electrons (see Fig. 3) [108]. The A electrons comoving with E_x get a pronounced energy gain up to $\gamma_e \sim 10^3$. The initially backward-moving B electrons are below the threshold, i.e., $p_x \sim -\gamma_0 < p_{\text{th}}^-$, but they are still injected, because the magnetic deflection $\mathbf{v} \times \mathbf{B}$ leads to an attractor effect in (ξ, p_x) space [109], which drags the electrons toward the degraded Hamiltonian $\Pi_{||}$ [see the red arrows in Fig. 3(c)] [85]. The C electrons are trapped by the E_x induced by assembling two stretched-out density strips behind the flowing focus position. The slingshot acceleration is distinguishable from the previously identified stochastic acceleration, where electrons tend to be repetitively rebounded by magnetic turbulence [73–75] and undergo Fermi-like stochastic energization [68–73]. Figure 3(d) manifests that the primary contribution of photon emission near the preturbulent interface originates from the slingshot electrons. The

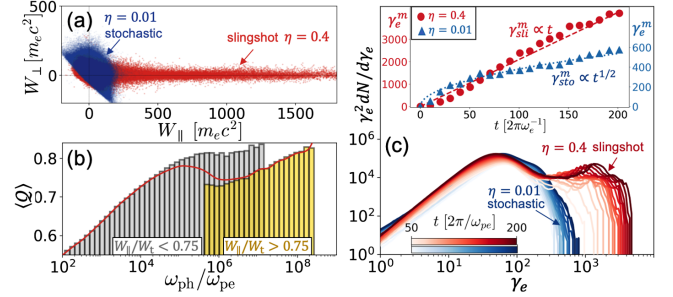


FIG. 4. (a) Distribution of $W_{||,\perp}$ at the emission moment. (b) $\langle Q \rangle$ versus ω_{ph} for photons associated with $W_{||}/W_t \leq 0.75$, where the red line reproduces the $\langle Q \rangle$ versus ω_{ph} in Fig. 1(c). (c) Time-evolved electron energy spectral $\gamma_e^2 dN/dy_e$. The inset displays the time-dependent electron maximum energy γ_e^m .

percentage of electrons undergoing a slingshot process is 0.39%.

In the search for a criterion distinguishing between the slingshot and stochastic electrons, we turn to the electron's longitudinal and transverse work $W_{||,\perp}$ [see Fig. 4(a)], where $W_{||} = -\int |e|E_x dx$, $W_{\perp} = -\int |e|E_y dy$, and $W_t = W_{||} + W_{\perp}$; the integrals are calculated from the beginning to the photon-emitting moment. The slingshot acceleration relies on E_x while the stochastic process is isotropic, meaning that the photon emission associated with $W_{||}/W_t \rightarrow 1$ ($W_{||}/W_t \rightarrow 0.5$) belongs to the slingshot (stochastic) mechanism [110]. Therefore, the condition of $W_{||}/W_t \leq 0.75$ is a reasonable criterion to distinguish the photon emission from the stochastic or slingshot mechanism. For the photons produced from the two mechanisms, both of their $\langle Q \rangle$ versus ω_{ph} [in Fig. 4(b)] are monotonically increasing as predicted by Eq. (1). However, the photon emission from the slingshot is shifted to the higher-frequency range compared with the stochastic scenario due to the enhanced energy of slingshot electrons [see Fig. 4(c)]. Therefore, the NMD of $\langle Q \rangle$ versus ω_{ph} comes from the combination between the high polarization degree stochastic photons and the low polarization degree slingshot photons around $\omega_{\text{ph}} \sim 10^6 \omega_{pe}$ [see Fig. 4(b)]. Near this frequency region, the emission of both mechanisms contributes.

The maximum slingshot energy γ_{sli}^m is approximated as $\gamma_{\text{sli}}^m \sim |e|\langle E_x \rangle \delta t / m_e c \sim \pi \sqrt{\eta \gamma_0} \omega_{pe} \delta t$ when the electron energy is far from the saturation $\gamma_e \ll p_{\text{th}}^+ \sim 10^6$. The energy gain of the stochastic process is estimated using the random walk model [105]: $\gamma_{\text{sto}}^m \sim 0.5(\omega_{pe,0} \delta t)^{1/2} \gamma_0^{3/4} \eta^{1/4}$ [85]. These estimates agree well with the simulation results [Fig. 4(c)]. Following γ_{sli}^m and γ_{sto}^m , the photon cutoff frequency ω_{ph}^m for the slingshot and stochastic mechanisms is predicted as $\omega_{\text{ph}}^{m,\text{sli}} \sim \gamma_{\text{sli}}^m B \propto \gamma_0^{3/2} \eta$ and $\omega_{\text{ph}}^{m,\text{sto}} \sim \gamma_{\text{sto}}^m B \propto \gamma_0^2 \eta^{1/2}$ [see Fig. 5(a)] with the magnetic field strength $B \propto \gamma_0^{1/2}$.

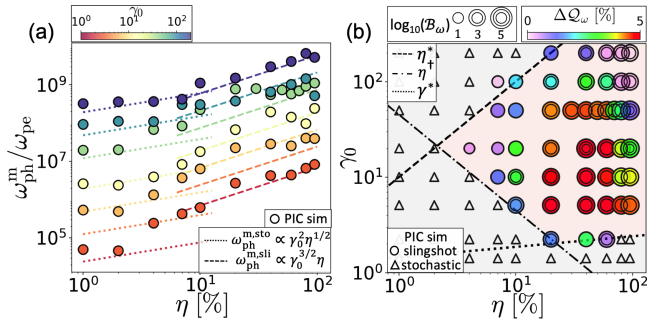


FIG. 5. (a) ω_{ph}^m versus η . (b) Dependence of ΔQ_ω and B_ω on η and γ_0 , where the circles (triangles) refer to the electron dynamics dominated by the slingshot (stochastic) mechanism.

Examining the NMD polarization features of the polarization dip ΔQ_ω and the bandwidth B_ω , we conclude that the high-frequency photon emission is dominated by the slingshot mechanism due to fulfilling three criteria: (i) The photon cutoff frequency originating from slingshot electrons is much higher than via the stochastic mechanism, i.e., $\omega_{\text{ph}}^{m,\text{sli}} \gg \omega_{\text{ph}}^{m,\text{sto}}$, reformulated as $\eta \gtrsim \eta^* = 0.01\gamma_0$; (ii) the number of the slingshot injected electron $N_e^{\text{sli}} \propto \langle E_x \rangle$ should be larger than the most energetic part of the stochastic electrons $N_e^{\text{sto}} \propto n_{pe0}$, rearranged as $\eta \gtrsim \eta^\dagger \propto \gamma_0^{-1}$; (iii) the saturation of the slingshot acceleration should be higher than the stochastic acceleration, i.e., $p_{\text{th}}^+ \gtrsim \gamma_{\text{sto}}^m$, expressed as $\gamma_0 \gtrsim \gamma^* = 2\eta^{1/9}$. The criteria of the slingshot dominance predicted by $\eta > \max\{\eta^*, \eta^\dagger\}$ and $\gamma > \gamma^*$ agrees well with the simulation results [see Fig. 5(b)]. The dependence of ΔQ_ω and B_ω on η and γ_0 in Fig. 5(b) confirms that the NMD of the polarization degree on photon energy is exclusively from the emission dominated by the slingshot mechanism.

In conclusion, inspecting the origin of unexpected polarization features of the photon radiation in the transient preturbulent RCS precursor, we have identified the electron slingshotlike acceleration mechanism, distinct from the well-known stochastic acceleration [68–72]. Our results have implications for both laboratory and astrophysical phenomena. The identified features of the transition region to turbulence, slingshot injection, and the photon polarization dependence could be actualized in laboratory astrophysics by using the combination of high-energy ion [111] and e^\pm beams [112]. Moreover, the slingshot electrons, escaping from the preturbulent region to enter the magnetic turbulent plasma [85], potentially behave as the prestage injection for the subsequent Fermi acceleration in long-term evolved RCSs [113]. Finally, the nontrivial photon polarization dynamics implies the necessity of revising the retrieval model for astrophysical magnetic configurations based on radiation features [79,80,114,115].

The original version of code EPOCH adapted here is funded by the United Kingdom Engineering and Physical

Sciences Research Council Grants No. EP/G054950/1, No. EP/G056803/1, No. EP/G055165/1, and No. EP/M022463/1. The authors thank Laurent Gremillet, Anatoly Spitkovsky, and Dmitri Uzdensky for the discussion regarding plasma stream instabilities, the initialization of RCS in PIC simulations, and the undetermined composition of astrophysical jets, respectively. The authors also thank the anonymous referees for their useful comments and suggestions. Z. G. thanks Zhi-Qiu Huang for the gained knowledge about the RCS generated following gamma-ray bursts.

*Present address: Department of Mechanical Engineering, Stanford University, Stanford, California 94305, USA. zgong92@stanford.edu; gong@mpi-hd.mpg.de
†k.hatsagortsyan@mpi-hd.mpg.de

- [1] R. Sagdeev, Cooperative phenomena and shock waves in collisionless plasmas, *Rev. Plasma Phys.* **4**, 23 (1966), <https://ui.adsabs.harvard.edu/abs/1966RvPP...4...23S/abstract>.
- [2] R. Courant and K. O. Friedrichs, *Supersonic Flow and Shock Waves* (Springer Science & Business Media, New York, 1999), Vol. 21.
- [3] L. D. Landau and E. M. Lifshitz, *Fluid Mechanics: Course of Theoretical Physics* (Pergamon press, Oxford, 2013), Vol. 6.
- [4] L. O. Silva, M. Marti, J. R. Davies, R. A. Fonseca, C. Ren, F. S. Tsung, and W. B. Mori, Proton shock acceleration in laser-plasma interactions, *Phys. Rev. Lett.* **92**, 015002 (2004).
- [5] L. Ji, B. Shen, X. Zhang, F. Wang, Z. Jin, X. Li, M. Wen, and J. R. Cary, Generating monoenergetic heavy-ion bunches with laser-induced electrostatic shocks, *Phys. Rev. Lett.* **101**, 164802 (2008).
- [6] F. Fiúza, A. Stockem, E. Boella, R. A. Fonseca, L. O. Silva, D. Haberberger, S. Tochitsky, C. Gong, W. B. Mori, and C. Joshi, Laser-driven shock acceleration of monoenergetic ion beams, *Phys. Rev. Lett.* **109**, 215001 (2012).
- [7] D. Haberberger, S. Tochitsky, F. Fiúza, C. Gong, R. A. Fonseca, L. O. Silva, W. B. Mori, and C. Joshi, Collisionless shocks in laser-produced plasma generate monoenergetic high-energy proton beams, *Nat. Phys.* **8**, 95 (2012).
- [8] H. Zhang, B. F. Shen, W. P. Wang, S. H. Zhai, S. S. Li, X. M. Lu, J. F. Li, R. J. Xu, X. L. Wang, X. Y. Liang, Y. X. Leng, R. X. Li, and Z. Z. Xu, Collisionless shock acceleration of high-flux quasimonoenergetic proton beams driven by circularly polarized laser pulses, *Phys. Rev. Lett.* **119**, 164801 (2017).
- [9] Y. Yao *et al.*, High-flux neutron generator based on laser-driven collisionless shock acceleration, *Phys. Rev. Lett.* **131**, 025101 (2023).
- [10] R. Betti, C. D. Zhou, K. S. Anderson, J. L. Perkins, W. Theobald, and A. A. Solodov, Shock ignition of thermonuclear fuel with high areal density, *Phys. Rev. Lett.* **98**, 155001 (2007).
- [11] L. J. Perkins, R. Betti, K. N. LaFortune, and W. H. Williams, Shock ignition: A new approach to high gain inertial confinement fusion on the national ignition facility, *Phys. Rev. Lett.* **103**, 045004 (2009).

- [12] C. Riconda, S. Weber, V. Tikhonchuk, and A. Héron, Kinetic simulations of stimulated raman backscattering and related processes for the shock-ignition approach to inertial confinement fusion, *Phys. Plasmas* **18**, 092701 (2011).
- [13] R. H. H. Scott, D. Barlow, W. Trickey, A. Ruocco, K. Glize, L. Antonelli, M. Khan, and N. C. Woolsey, Shock-augmented ignition approach to laser inertial fusion, *Phys. Rev. Lett.* **129**, 195001 (2022).
- [14] G. Gregori, A. Ravasio, C. Murphy, K. Schaar, A. Baird, A. Bell, A. Benuzzi-Mounaix, R. Bingham, C. Constantin, R. Drake *et al.*, Generation of scaled protogalactic seed magnetic fields in laser-produced shock waves, *Nature (London)* **481**, 480 (2012).
- [15] N. Kugland, D. Ryutov, P. Chang, R. Drake, G. Fiksel, D. Froula, S. Glenzer, G. Gregori, M. Grosskopf, M. Koenig *et al.*, Self-organized electromagnetic field structures in laser-produced counter-streaming plasmas, *Nat. Phys.* **8**, 809 (2012).
- [16] W. Fox, G. Fiksel, A. Bhattacharjee, P.-Y. Chang, K. Germaschewski, S. X. Hu, and P. M. Nilson, Filamentation instability of counterstreaming laser-driven plasmas, *Phys. Rev. Lett.* **111**, 225002 (2013).
- [17] C. Huntington, F. Fiuza, J. Ross, A. Zylstra, R. Drake, D. Froula, G. Gregori, N. Kugland, C. Kuranz, M. Levy *et al.*, Observation of magnetic field generation via the Weibel instability in interpenetrating plasma flows, *Nat. Phys.* **11**, 173 (2015).
- [18] C. K. Li, V. T. Tikhonchuk, Q. Moreno, H. Sio, E. d'Humieres, X. Ribeyre, P. Korneev, S. Atzeni, R. Betti, A. Birkel *et al.*, Collisionless shocks driven by supersonic plasma flows with self-generated magnetic fields, *Phys. Rev. Lett.* **123**, 055002 (2019).
- [19] C. Ruyer, S. Bolaños, B. Albertazzi, S. Chen, P. Antici, J. Böker, V. Dervieux, L. Lancia, M. Nakatsutsumi, L. Romagnani *et al.*, Growth of concomitant laser-driven collisionless and resistive electron filamentation instabilities over large spatiotemporal scales, *Nat. Phys.* **16**, 983 (2020).
- [20] F. Fiuza, G. Swadling, A. Grassi, H. Rinderknecht, D. Higginson, D. Ryutov, C. Bruulsema, R. Drake, S. Funk, S. Glenzer *et al.*, Electron acceleration in laboratory-produced turbulent collisionless shocks, *Nat. Phys.* **16**, 916 (2020).
- [21] K. Koyama, R. Petre, E. Gotthelf, U. Hwang, M. Matsuura, M. Ozaki, and S. Holt, Evidence for shock acceleration of high-energy electrons in the supernova remnant SN1006, *Nature (London)* **378**, 255 (1995).
- [22] R. Diesing and D. Caprioli, Spectrum of electrons accelerated in supernova remnants, *Phys. Rev. Lett.* **123**, 071101 (2019).
- [23] M. Aguilar, L. A. Cavazonza, G. Ambrosi, L. Arruda, N. Attig *et al.*, Towards understanding the origin of cosmic-ray positrons, *Phys. Rev. Lett.* **122**, 041102 (2019).
- [24] M. Aguilar, L. A. Cavazonza, B. Alpat, G. Ambrosi, L. Arruda, A. Barrau *et al.*, Towards understanding the origin of cosmic-ray electrons, *Phys. Rev. Lett.* **122**, 101101 (2019).
- [25] K. Fang, M. Kerr, R. Blandford, H. Fleischhack, and E. Charles, Evidence for peV proton acceleration from Fermi-Lat observations of SNR g 106.3 + 2.7, *Phys. Rev. Lett.* **129**, 071101 (2022).
- [26] J. G. Kirk, Y. Lyubarsky, and J. Petri, The theory of pulsar winds and nebulae, in *Neutron Stars and Pulsars* (Springer, New York, 2009), pp. 421–450, [10.1007/978-3-540-76965-1_16](https://doi.org/10.1007/978-3-540-76965-1_16).
- [27] G. E. Romero, M. Boettcher, S. Markoff, and F. Tavecchio, Relativistic jets in active galactic nuclei and microquasars, *Space Sci. Rev.* **207**, 5 (2017).
- [28] T. Piran, The physics of gamma-ray bursts, *Rev. Mod. Phys.* **76**, 1143 (2005).
- [29] E. Troja *et al.*, A nearby long gamma-ray burst from a merger of compact objects, *Nature (London)* **612**, 228 (2022).
- [30] J. C. Rastinejad, N. R. Tanvir *et al.*, A kilonova following a long-duration gamma-ray burst at 350 mpc, *Nature (London)* **612**, 223 (2022).
- [31] A. Mei, B. Banerjee, G. Oganessian *et al.*, Giga-electronvolt emission from a compact binary merger, *Nature (London)* **612**, 236 (2022).
- [32] J. Yang, S. Ai, B.-B. Zhang, B. Zhang, Z.-K. Liu, X. I. Wang, Y.-H. Yang, Y.-H. Yin, Y. Li, and H.-J. Lü, A long-duration gamma-ray burst with a peculiar origin, *Nature (London)* **612**, 232 (2022).
- [33] S. Woosley and J. Bloom, The supernova–gamma-ray burst connection, *Annu. Rev. Astron. Astrophys.* **44**, 507 (2006).
- [34] D. Grošelj, L. Sironi, and A. M. Beloborodov, Microphysics of relativistic collisionless electron-ion-positron shocks, *Astrophys. J.* **933**, 74 (2022).
- [35] C. Thompson and P. Madau, Relativistic winds from compact gamma-ray sources. II. Pair loading and radiative acceleration in gamma-ray bursts, *Astrophys. J.* **538**, 105 (2000).
- [36] P. Mészáros, E. Ramirez-Ruiz, and M. Rees, $e \pm$ pair cascades and precursors in gamma-ray bursts, *Astrophys. J.* **554**, 660 (2001).
- [37] A. M. Beloborodov, Radiation front sweeping the ambient medium of gamma-ray bursts, *Astrophys. J.* **565**, 808 (2002).
- [38] A. Gruzinov, Gamma-ray burst phenomenology, shock dynamo, and the first magnetic fields, *Astrophys. J.* **563**, L15 (2001).
- [39] M. V. Medvedev and A. Loeb, Generation of magnetic fields in the relativistic shock of gamma-ray burst sources, *Astrophys. J.* **526**, 697 (1999).
- [40] M. Honda, J. Meyer-ter Vehn, and A. Pukhov, Collective stopping and ion heating in relativistic-electron-beam transport for fast ignition, *Phys. Rev. Lett.* **85**, 2128 (2000).
- [41] L. Silva, R. Fonseca, J. Tonge, J. Dawson, W. Mori, and M. Medvedev, Interpenetrating plasma shells: Near-equipartition magnetic field generation and nonthermal particle acceleration, *Astrophys. J.* **596**, L121 (2003).
- [42] A. Bell, Turbulent amplification of magnetic field and diffusive shock acceleration of cosmic rays, *Mon. Not. R. Astron. Soc.* **353**, 550 (2004).
- [43] A. Bret, M.-C. Firpo, and C. Deutsch, Characterization of the initial filamentation of a relativistic electron beam passing through a plasma, *Phys. Rev. Lett.* **94**, 115002 (2005).
- [44] F. Califano, D. Del Sarto, and F. Pegoraro, Three-dimensional magnetic structures generated by the development of the filamentation (Weibel) instability in the relativistic regime, *Phys. Rev. Lett.* **96**, 105008 (2006).

- [45] A. Bret, L. Gremillet, D. Bénisti, and E. Lefebvre, Exact relativistic kinetic theory of an electron-beam–plasma system: Hierarchy of the competing modes in the system-parameter space, *Phys. Rev. Lett.* **100**, 205008 (2008).
- [46] Z. Gong, K. Z. Hatsagortsyan, and C. H. Keitel, Electron polarization in ultrarelativistic plasma current filamentation instabilities, *Phys. Rev. Lett.* **130**, 015101 (2023).
- [47] E. S. Weibel, Spontaneously growing transverse waves in a plasma due to an anisotropic velocity distribution, *Phys. Rev. Lett.* **2**, 83 (1959).
- [48] F. Fiúza, R. A. Fonseca, J. Tonge, W. B. Mori, and L. O. Silva, Weibel-instability-mediated collisionless shocks in the laboratory with ultraintense lasers, *Phys. Rev. Lett.* **108**, 235004 (2012).
- [49] C. Ruyer, L. Gremillet, G. Bonnaud, and C. Riconda, Analytical predictions of field and plasma dynamics during nonlinear Weibel-mediated flow collisions, *Phys. Rev. Lett.* **117**, 065001 (2016).
- [50] A. Marcowith, A. Bret, A. Bykov, M. E. Dieckman, L. O. Drury, B. Lembège, M. Lemoine, G. Morlino, G. Murphy, G. Pelletier *et al.*, The microphysics of collisionless shock waves, *Rep. Prog. Phys.* **79**, 046901 (2016).
- [51] A. Grassi, M. Grech, F. Amiranoff, A. Macchi, and C. Riconda, Radiation-pressure-driven ion Weibel instability and collisionless shocks, *Phys. Rev. E* **96**, 033204 (2017).
- [52] V. Zhdankin, G. R. Werner, D. A. Uzdensky, and M. C. Begelman, Kinetic turbulence in relativistic plasma: From thermal bath to nonthermal continuum, *Phys. Rev. Lett.* **118**, 055103 (2017).
- [53] M. Lemoine, L. Gremillet, G. Pelletier, and A. Vanthieghem, Physics of Weibel-mediated relativistic collisionless shocks, *Phys. Rev. Lett.* **123**, 035101 (2019).
- [54] A. Bohdan, M. Pohl, J. Niemiec, P. J. Morris, Y. Matsumoto, T. Amano, M. Hoshino, and A. Sulaiman, Magnetic field amplification by the Weibel instability at planetary and astrophysical shocks with high mach number, *Phys. Rev. Lett.* **126**, 095101 (2021).
- [55] E. Fermi, On the origin of the cosmic radiation, *Phys. Rev.* **75**, 1169 (1949).
- [56] E. Fermi, Galactic magnetic fields and the origin of cosmic radiation, *Astrophys. J.* **119**, 1 (1954).
- [57] A. Bell, The acceleration of cosmic rays in shock fronts–I, *Mon. Not. R. Astron. Soc.* **182**, 147 (1978).
- [58] A. Spitkovsky, Particle acceleration in relativistic collisionless shocks: Fermi process at last?, *Astrophys. J.* **682**, L5 (2008).
- [59] V. Petrosian, Stochastic acceleration by turbulence, *Space Sci. Rev.* **173**, 535 (2012).
- [60] Y. Matsumoto, T. Amano, T. Kato, and M. Hoshino, Stochastic electron acceleration during spontaneous turbulent reconnection in a strong shock wave, *Science* **347**, 974 (2015).
- [61] L. Sironi, U. Keshet, and M. Lemoine, Relativistic shocks: Particle acceleration and magnetization, *Space Sci. Rev.* **191**, 519 (2015).
- [62] Y. Matsumoto, T. Amano, T. N. Kato, and M. Hoshino, Electron surfing and drift accelerations in a Weibel-dominated high-mach-number shock, *Phys. Rev. Lett.* **119**, 105101 (2017).
- [63] L. Comisso and L. Sironi, Particle acceleration in relativistic plasma turbulence, *Phys. Rev. Lett.* **121**, 255101 (2018).
- [64] V. Zhdankin, D. A. Uzdensky, G. R. Werner, and M. C. Begelman, Electron and ion energization in relativistic plasma turbulence, *Phys. Rev. Lett.* **122**, 055101 (2019).
- [65] L. Comisso and L. Sironi, Pitch-angle anisotropy controls particle acceleration and cooling in radiative relativistic plasma turbulence, *Phys. Rev. Lett.* **127**, 255102 (2021).
- [66] M. Lemoine, First-principles fermi acceleration in magnetized turbulence, *Phys. Rev. Lett.* **129**, 215101 (2022).
- [67] T. Amano, Y. Matsumoto, A. Bohdan, O. Kobzar, S. Matsukiyo, M. Oka, J. Niemiec, M. Pohl, and M. Hoshino, Nonthermal electron acceleration at collisionless quasi-perpendicular shocks, *Rev. Mod. Plasma Phys.* **6**, 29 (2022).
- [68] M. Milosavljević and E. Nakar, The cosmic-ray precursor of relativistic collisionless shocks: A missing link in gamma-ray burst afterglows, *Astrophys. J.* **651**, 979 (2006).
- [69] A. Spitkovsky, On the structure of relativistic collisionless shocks in electron-ion plasmas, *Astrophys. J.* **673**, L39 (2007).
- [70] T. Haugbølle, Three-dimensional modeling of relativistic collisionless ion–electron shocks, *Astrophys. J. Lett.* **739**, L42 (2011).
- [71] I. Plotnikov, G. Pelletier, and M. Lemoine, Particle transport and heating in the microturbulent precursor of relativistic shocks, *Mon. Not. R. Astron. Soc.* **430**, 1280 (2013).
- [72] N. Naseri, S. Bochkarev, V. Bychenkov, V. Khudik, and G. Shvets, Electron energization dynamics in interaction of self-generated magnetic vortices in upstream of collisionless electron/ion shocks, *Sci. Rep.* **12**, 7327 (2022).
- [73] N. Naseri, S. Bochkarev, P. Ruan, V. Y. Bychenkov, V. Khudik, and G. Shvets, Growth and propagation of self-generated magnetic dipole vortices in collisionless shocks produced by interpenetrating plasmas, *Phys. Plasmas* **25**, 012118 (2018).
- [74] J. R. Peterson, S. Glenzer, and F. Fiúza, Magnetic field amplification by a nonlinear electron streaming instability, *Phys. Rev. Lett.* **126**, 215101 (2021).
- [75] J. R. Peterson, S. Glenzer, and F. Fiúza, Magnetic field amplification by a plasma cavitation instability in relativistic shock precursors, *Astrophys. J. Lett.* **924**, L12 (2022).
- [76] I. Bartos and M. Kowalski, *Multimessenger* (IOP Publishing, Bristol, 2017).
- [77] P. Mészáros, D. B. Fox, C. Hanna, and K. Murase, Multimessenger astrophysics, *Nat. Rev. Phys.* **1**, 585 (2019).
- [78] E. Komatsu, New physics from the polarized light of the cosmic microwave background, *Nat. Rev. Phys.* **4**, 452 (2022).
- [79] K. Akiyama, J. C. Algaba, A. Alberdi, W. Alef, R. Anantua, K. Asada, R. Azulay, A.-K. Bacsko, D. Ball, M. Baloković *et al.*, First M87 Event Horizon Telescope Results. VIII. Magnetic field structure near the event horizon, *Astrophys. J. Lett.* **910**, L13 (2021).
- [80] N. Bucciantini, R. Ferrazzoli, M. Bachetti, J. Rankin, N. Di Lalla, C. Sgrò, N. Omodei, T. Kitaguchi, T. Mizuno, S. Gunji *et al.*, Simultaneous space and phase resolved x-ray polarimetry of the crab pulsar and nebula, *Nat. Astron.*, **7**, 602 (2023).

- [81] M. Gedalin, M. A. Balikhin, and D. Eichler, Efficient electron heating in relativistic shocks and gamma-ray-burst afterglow, *Phys. Rev. E* **77**, 026403 (2008).
- [82] R. Kumar, D. Eichler, and M. Gedalin, Electron heating in a relativistic, Weibel-unstable plasma, *Astrophys. J.* **806**, 165 (2015).
- [83] A. Vanthieghem, M. Lemoine, and L. Gremillet, Origin of intense electron heating in relativistic blast waves, *Astrophys. J. Lett.* **930**, L8 (2022).
- [84] T. Arber, K. Bennett, C. Brady, A. Lawrence-Douglas, M. Ramsay, N. Sircombe, P. Gillies, R. Evans, H. Schmitz, A. Bell *et al.*, Contemporary particle-in-cell approach to laser-plasma modelling, *Plasma Phys. Controlled Fusion* **57**, 113001 (2015).
- [85] See Supplemental Material at <http://link.aps.org/supplemental/10.1103/PhysRevLett.131.225101> for the discussion on the model of photon polarization implemented in PIC code, the analytical derivation for electron dynamics in backward-flowing focus and slingshot injection, extra detailed simulation results, and the electron stochastic acceleration based on the random walk model. Supplemental Material includes Refs. [86–95].
- [86] J. D. Jackson, *Classical Electrodynamics* (John Wiley & Sons, USA, 1999).
- [87] R. Duclous, J. G. Kirk, and A. R. Bell, Monte Carlo calculations of pair production in high-intensity laser-plasma interactions, *Plasma Phys. Controlled Fusion* **53**, 015009 (2010).
- [88] N. Elkina, A. Fedotov, I. Y. Kostyukov, M. Legkov, N. Narozhny, E. Nerush, and H. Ruhl, Qed cascades induced by circularly polarized laser fields, *Phys. Rev. Accel. Beams* **14**, 054401 (2011).
- [89] C. Ridgers, J. G. Kirk, R. Duclous, T. Blackburn, C. Brady, K. Bennett, T. Arber, and A. Bell, Modelling gamma-ray photon emission and pair production in high-intensity laser-matter interactions, *J. Comput. Phys.* **260**, 273 (2014).
- [90] A. Gonoskov, S. Bastrakov, E. Efimenko, A. Ilderton, M. Marklund, I. Meyerov, A. Muraviev, A. Sergeev, I. Surmin, and E. Wallin, Extended particle-in-cell schemes for physics in ultrastrong laser fields: Review and developments, *Phys. Rev. E* **92**, 023305 (2015).
- [91] Z. Gong, K. Z. Hatsagortsyan, and C. H. Keitel, Deciphering *in situ* electron dynamics of ultrarelativistic plasma via polarization pattern of emitted γ -photons, *Phys. Rev. Res.* **4**, L022024 (2022).
- [92] K. Yokoya and P. Chen, Yokoya, 'User's Manual of CAIN', Version (2003).
- [93] L. Sironi and A. Spitkovsky, Synthetic spectra from particle-in-cell simulations of relativistic collisionless shocks, *Astrophys. J.* **707**, L92 (2009).
- [94] D. Jordan and P. Smith, *Nonlinear Ordinary Differential Equations: An Introduction for Scientists and Engineers* (OUP, Oxford, 2007).
- [95] L. Sironi, A. Spitkovsky, and J. Arons, The maximum energy of accelerated particles in relativistic collisionless shocks, *Astrophys. J.* **771**, 54 (2013).
- [96] See the animation for the detailed electron density, electron motion, and photon emission for the case of $\eta = 0.4$ (animation_fig1a_density_eta040.gif).
- [97] See the animation for the detailed electron density, electron motion, and photon emission for the case of $\eta = 0.01$ (animation_fig1a_density_eta001.gif).
- [98] See the animation for the analytically predicted electron trajectories of the backward-flowing focus (animation_fig2a.gif).
- [99] See the animation for the simulated electron trajectories of the backward-flowing focus (animation_fig2b.gif).
- [100] See the animation for the analytically predicted electron evolution in the transverse phase space (animation_fig2c_analytical.gif).
- [101] W. H. McMaster, Polarization and the stokes parameters, *Am. J. Phys.* **22**, 351 (1954).
- [102] A. Vulpiani, F. Cecconi, and M. Cencini, *Chaos: From Simple Models to Complex Systems* (World Scientific, Singapore, 2009), Vol. 17.
- [103] See the animation for the detailed evolution of δr and electron motion at $\omega_{pet}/2\pi \sim 45$ (animation_fig2d_1.gif).
- [104] See the animation for the detailed evolution of δr and electron motion at $\omega_{pet}/2\pi \sim 70$ (animation_fig2d_2.gif).
- [105] O. C. Ibe, *Elements of Random Walk and Diffusion Processes* (John Wiley & Sons, New York, 2013).
- [106] See the animation for the detailed evolution of δr and electron motion at $\omega_{pet}/2\pi > 130$ (animation_fig2d_3.gif).
- [107] See the animation for the detailed electron dynamics and photon emission (animation_shining_eta040.gif).
- [108] See the animation for the detailed slingshot injection process (animation_fig3a.gif).
- [109] M. W. Hirsch, S. Smale, and R. L. Devaney, *Differential Equations, Dynamical Systems, and an Introduction to Chaos* (Academic Press, New York, 2012).
- [110] In the PIC simulations, the work $W_{\parallel,\perp}$ could be recorded on the photon particle. When a photon is emitted from its parent electron, it inherits the work value $W_{\parallel,\perp}$ from the electron at that moment. Therefore, each photon would have an attribute of its parental electron's work contribution $W_{\parallel,\perp}$. This is convenient for presenting the correlation between the photon polarization and the work contribution (i.e., the acceleration mechanism).
- [111] P. Muggli *et al.* (AWAKW Collaboration), Physics to plan AWAKE Run 2, *J. Phys. Conf. Ser.* **1596**, 012008 (2020).
- [112] H. Chen and F. Fiuza, Perspectives on relativistic electron-positron pair plasma experiments of astrophysical relevance using high-power lasers, *Phys. Plasmas* **30**, 020601 (2023).
- [113] R. Blandford and D. Eichler, Particle acceleration at astrophysical shocks: A theory of cosmic ray origin, *Phys. Rep.* **154**, 1 (1987).
- [114] H. Zhang, W. Deng, H. Li, and M. Böttcher, Polarization signatures of relativistic magnetohydrodynamic shocks in the blazar emission region. I. Force-free helical magnetic fields, *Astrophys. J.* **817**, 63 (2016).
- [115] L. Sironi, I. Plotnikov, J. Näätä, and A. M. Beloborodov, Coherent electromagnetic emission from relativistic magnetized shocks, *Phys. Rev. Lett.* **127**, 035101 (2021).